The limitations and pitfalls in clinical implications of Bragg's peak: A theoretical SRIM – TRIM model of human breast tumor

Marwan S.M. Al-Nimer and Zainab Wahbee Abdul Lateef
Department of Pharmacology/College of Medicine/Al-Mustansiriya University
Department of Physiology/College of Medicine/Al-Mustansiriya University

الخلاصة

تعد معالجة حزمة البروتون فريدة لأنها تسمح بوضع طاقتها الأيونية في عمق محدد مع تبعثر ضئيل جدا في الطاقة والتي تعرف بقمة براك. هدفت الدراسة الى التقصي عن الهفوات التي يمكن ان تحصل عند تطبيق قمة براك لنموذج نظري لأورام الثدي في الانسان. تم استعمال برنامج سرم – ترم طبعة ١٩٩٨ و٢٠٠٣ وتم تصميم نموذج لسرطان الثدي بحيث تخترق الايونات (الهيدروجين او الكاربون) وبطاقات مختلفة طبقات الجلد والشحم وانسجة الثدي الطبيعية ونسيج ورم في الثدي ذو كثافات مختلفة. اظهرت النتائج ان الطاقة المكبوحة للكاربون هي اكبر من الهيدروجين وتتناسب طرديا مع كثافة النسيج. وتناسب المدى الأفقي عند اختراق الأيونات مع الطاقة المسلطة وقد تدنى اقتحام ايونات الهيدروجين بزيادة كثافة نسيج الورم في حين كانت الطاقة المفقودة في الورم عالية مع تشعيع الكاربون. وقد تسبب التشعيع الأيوني الذي تناسب طرديا مع الطاقة المسلطة وعكسيا مع كتلة الورم في تلف الورم . نستنتج من هذه الدراسة انه بالأمكان الحصول على قمة براك وتطبيقه في معالجة اورام الثدي اذا ما اخذ بنظر الاعتبار كثافة او كتلة الورم ، و موضع الورم في النسيج الطبيعي و طبيعة الأيون المشعع والطاقة المسلطة مجتمعة.

ABSTRACT

Proton beam therapy is unique because it allows for minimal scattering as particulate beam pass through tissue and deposing ionizing energy at precise depth i.e. Bragg peak. This study is aimed to investigate the limitations and pitfalls in clinical application of Bragg peak in theoretical model of human breast tumor. The Microsoft; "The Stopping and Range of Ions in Matter (SRIM)" version 1998, and 2003 was used. A model of breast tumor was designed and the projection of irradiated ions (hydrogen or carbon) crossed multi-layers including skin, adipose tissue, normal and abnormal breast tissues of different densities. The results showed that the stopping power of carbon ions was higher than corresponding hydrogen ions and proportionally increased with tissue density. The longitudinal range was directly correlated with acceleration potential energy for both hydrogen and carbon ions. The straggling of the hydrogen ions and to lesser extent the carbon ions tended to be declined, for each accelerated potential, with increment in density of breast tissue. The energy loss was higher with carbon ions compared with hydrogen ions. Irradiation with hydrogen or carbon ions resulted in breast tissue damage which was proportionally related to the accelerated potentials and inversely with target density. The damaging effect of carbon ions was inferior to that of hydrogen ions. It concludes that typical Bragg's peak can be achieved when the density of irradiated tissue , the localization of abnormal tissue , the type of ions radiation and the acceleration potentials are taken collectively in consideration.

Key words: Breast tumor, Bragg peak

INTRODUCTION

The concept of proton therapy was first developed by, the father of proton therapy, Dr. Robert Rathbun Wilson in 1946 (1). In 1954, the university of Berkeley began using proton technology after the construction of a cyclotron to treat cancer patient. In the United States there are few facilities offering proton therapy. The therapeutic use of protons (or helium ions) is produced by an accelerator; cyclotron, synchrotron, synchrocyclotron or linear (2). This type of

radiation is unique because it allows for minimal scattering as particulate beam pass through tissue and deposing ionizing energy at precise depth i.e. Bragg peak, which was described by William Bragg over 100 years (3,4). The heavy particles appear to continuously slow down gradually losing their energy along an unaltered linear path. Protons pass near orbiting electrons pulling them out of their orbits causing ionization (5). These processes end with the heating of the absorber (i.e. the target) through atom and of the molecule. The real advantages of proton therapy could not be realized until imaging systems; computerized tomography, magnetic resonance image, positron emission tomography were invented that could precisely located the tumor lesion (6).

The exact depth to which protons penetrate, and at which the Bragg peak occurs, is dependent on the energy of the proton beam. This energy can be very precisely controlled the place of the Bragg peak within a tumor or other tissue that are targeted to receive the radiation dose. The energy is inversely proportioned with stopping power. The other influencing factors include the electron mass, the charge and the target density. The electron is much faster than the alpha particles due to its smaller mass, therefore, the electron has less time to spread near orbital electrons. This reduces the effect of Coulomb interactions (hence stopping power) and increase range. The more charge or density, the more stopping power and the lower range. Protons have physical advantages over gamma rays and X-rays when it comes to sparing normal tissue and to treat irregular shaped lesions with awkward configurations near critical structures (7). The use of proton beam radiation therapy (PBRT) has been studied most extensively in terms of clinical effectiveness and safety for the treatment of uveal (ocular) melanoma, pituitary adenoma, and intracranial arterio-venous malformation where open surgery is not an option and conventional radiation therapy may not be appropriate (8,9). Also it is indicated for carcinoma of prostate, head and neck tumors etc.. (10,11).

This study is aimed to demonstrate the limitations and pitfalls in clinical application of Bragg peak in theoretical model of human breast tumor if the management of breast cancer is carried on by proton beams (hydrogen or carbon ions).

MATERIALS AND METHODS

This study was conducted in Department of Physiology/Medical Physics in cooperation with Department of Pharmacology, College of Medicine, Al-Mustansiriya University in Baghdad, Iraq during 2009. The Microsoft "The Stopping and Range of Ions in Matter (SRIM)" version 1998, and 2003 was used. A model of breast tumor located 27 mm from the skin was persumed. Therefore, projection of protons passed through skin (presumed as normal healthy skin of 2mm), subcutaneous and mammary adipose tissues (presumed 5 mm) and the pre-tumor healthy mammary tissues of 20 mm. The specifications

of each layer and the breast tumors of different densities were seen in table 1. The effectiveness of proton beam therapy was studied using fixed localization of tumors but differed in their densities (1.5, 2.0 and 2.5 g/cm^3) irradiated by acceleration potential of 60, 70, 80 and 90 MeV. The following variables were considered in assessment the effectiveness and the hazard of proton:

a. Hydrogen ion (1 amu) projected to the target tissue at 0 angle i.e. perpendicular to the tumor.

b. The transmitted ions, scattered ions, the range and the straggle of ions in longitudinal (X) lateral (Y), radial (Z) projections.

c. Vacancy/ion,

d. Percent of energy loss in ion ionization

e. A symmetrical distribution of energy losses of particles i.e. straggling

f. Phonens

g. Ion effective charge, fractional effective charge, vacancies energy loss and energy loss (eVA) for 25000 electrons were considered in assessment of proton beam therapy.

In another series of experiments , the carbon ions (for 10000 electrons) instead of hydrogen ions are delivered at acceleration potential of 600, 700, 800 and 900 MeV to the breast tissue of 0.99 g/cm^3 density.

The stopping power (S) is given by:

S= - dE/dx

The quantity of S (keV/μ) is referred to specific energy loss

E: charged particle kinetic energy

-dE: the energy increment lost in infinitesimal material thickness (dx)

The specific energy loss is expressed by Bethe-Bloch formula (12,13).

For heavy charged particle:

$$-\frac{dE}{dx} = \frac{4\pi e^4 z^2}{m_o v^2} NB$$

Where

$$B = Z\left[\ln\frac{2m_o v^2}{I} - \ln\left(1-\frac{v^2}{c^2}\right) - \frac{v^2}{c^2}\right]$$

With the following definitions:

V velocity of the charged particle
ze charge of the charged particle
N number density of absorber atoms
Z atomic number of absorber atoms
m electron rest mass
e electron charge
I A parameter, treated as experimentally determined, representing average
excitation and ionization potential

B is known as the stopping number (atomic number scaled for stopping)

Bethe-Bloch formula for electrons :

$-dE/dx = (2\pi e^4 / m_o v^2) NB$

$$B=Z\left[\ln \frac{m_o v^2 T}{2I^2(1-\beta^2)} - (ln2)\left(2\sqrt{1-\beta^2} - 1 + \beta^2\right) + 1 - \beta^2 + \frac{1}{8}\left(1-\sqrt{1-\beta^2}\right)^2\right]$$

Where $\beta = \frac{v}{c}$

The total stopping power for electron can be given as a combination of collisional (inelastic collision with atomic electrons) and radiative (inelastic collision with nucleous) types of interaction; (Bremsstrahlung)

[dE/dx] total = [dE/dx]collision + [dE/dx] radiative

For heavy particles, orbital electron interactions are only considered since the probability of nuclear interaction resulting in energy loss is much smaller.

$$-\left(\frac{dE}{dx}\right)_r = \frac{NTZ(Z+1)e^4}{137 m_0^2 c^4}\left(4\ ln\frac{2T}{m_0 c^2} - \frac{4}{3}\right)$$

The percent of the energy loss goes to emitted rays is expressed by:

$$(\frac{dE}{dx})_r / (\frac{dE}{dx})total = EZ/1000$$

where E is in MeV, where Z is the atomic number of the absorber.

The range of a charged particle can be derived from stopping power formula:

$$R = \int_E^0 dx(cm) = \int_E^0 \frac{dE}{dE} dx = -\int_0^E \frac{1}{dE/dx} dE = \int_0^E \frac{dE}{S}$$

The summal distance elements as kinetic energy goes from *E* down to 0 is the total distance along the incident direction, or the range.

The lattice binding energy was 1.5 eV while the surface binding energy was 4.0 eV The displacement energy for each atom ; H (hydrogen), C (carbon), N (nitrogen), O (oxygen), Na (sodium), Mg (magnesium), P (phosphorus), S (sulphur), Cl (chloride), K (potassium), or Ca (calcium) or was 15 eV. The total target vacancies are depended on the accelerated potential and their energy loss was calculated by: Total target vacancies x binding energy (i.e. 1.5 eV). The Microsoft "The Stopping and Range of Ions in Matter (SRIM)" version 1998, and 2003 calculate the above variables and the lay out computerized data were obtained. Microsoft Excel 2003 was used for calculations and figures plotting.

RESULTS AND DISCUSSION

Figure 1 shows the stopping power of hydrogen ions in the skin and adipose tissue which differed from the stopping power of carbon ions. At the acceleration potential of 14 MeV, the stopping power of hydrogen at the distal end of the skin i.e. 2mm was 3.832 keV/µ while the stopping power of carbon ions was 927.4 keV/µ at longitudinal range of 5.61µ with acceleration potential of 4 MeV. Comparative results were obtained with adipose tissue. The stopping powers of hydrogen ions were 2.513 and 2.324 keV/µ for longitudinal ranges 4.39 and 5.21 mm at acceleration potentials of 20 and 22 MeV respectively. Again the stopping power of carbon ions was higher than corresponding hydrogen ions. It was 858.7 kev/ions at longitudinal range of 4.02µ with acceleration potential of 2.4 MeV.

In the breast tissue the stopping power of carbon ions were increased with increasing breast tissue density. It amounted 87.83, 1337, 1795, and 2244 kev/ion for breast tissue density of 0.99, 1.5, 2.0 and 2.5 g/cm^3 respectively [Fig.2].The stopping powers of hydrogen ions were 1.091, 1.653, 2.204 and 2.587 for corresponding breast mass density [Fig.2]. The longitudinal range was directly correlated with acceleration potential energy for both hydrogen and carbon ions but the depth tissue penetration was so lesser with carbon ions compared with than that observed with hydrogen ions [Fig 3]. From figure 3, the calculated energy for 1 micron and 1000 micron tissue penetration was 28.57 MeV and 32.50 MeV for carbon and hydrogen ions respectively. The interesting observation is the ability of hydrogen ions to deposit their energies in abnormal breast tissue (i.e. of different densities) that embedded in normal breast tissues with minimal effect of radiation to the normal breast tissue [Fig 4 A]. The energy deposited by carbon ions were superficial i.e. the Bragg's peak of abnormal breast tissue was shifted down to the normal breast tissue [Fig 4B].

The straggling of hydrogen ions whether longitudinal, radial, or lateral tended to be declined, for each accelerated potential, with increment in density of breast tissue [Tables 2-5], while the ion straggling was proportionally increased with increasing accelerated potential for each density [Tables 2-5].

The same finding was observed with carbon ions but to a lesser degree than that observed with hydrogen ions [Table 6]. For example the longitudinal straggling of hydrogen ion at 60 MeV acceleration potential was 1.269% (386µ/30.4 mm) compared with 0.32 (27.4 µ/7.48mm) at 600 MeV acceleration potential for carbon ions. The vacancies of the target was not differed for each accelerated potential when the tissue density was changed. In each breast tissue with specific density the vacancies were proportionally increased with high accelerated energy [Tables 2-6]. Table 7 shows the total energy loss in respect to the target vacancies. Taking in consideration the magnitude of accelerated potential and the counted electrons, the energy loss was higher with carbon ions compared with hydrogen ions. The shape of Bragg's peaks were statistically determined by the skewness and the kurtosis. Therefore, it is expected to find

several shapes according to the results of skewness and kurtosis listed in Tables2-6.

The electron stopping power of irradiated hydrogen to each atom of breast tissue was higher than that irradiated with carbon ions at all studied accelerated energies [Tables 8 and 9] while the picture is reversed with the nuclear stopping power. Moreover the ion effective charge as well as the fractional effective charge remained constant at different accelerated potentials with carbon ions but they fluctuated with hydrogen ions [Tables 8 & 9]. From the above data, the damaged breast tissue volume or mass were calculated. Table 10 shows that irradiation with hydrogen or carbon ions resulted in breast tissue damage which was proportionally related to the accelerated potentials and inversely with target density. The damaging effect of carbon ions was inferior to that of hydrogen ions.

The results of this study demonstrate that both hydrogen and carbon ions radiation produce ionization density in the Bragg region but their behaviors are differed. For the treatment purposes the position of Bragg peak needs to be spread out to cover the tumor volume and the production of such a spread out Bragg peak results in a build up in the spread out Bragg peak relative to the plateau (14). In this work the spread out Bragg peak is well demonstrated with hydrogen ions compared with carbon ions radiation (15). The width of Bragg peak for hydrogen and carbon ions in human tissues was less than the typical width of 8 mm for 177 MeV proton beam. In this study the Bragg curve of carbon ions radiation is differed from that of hydrogen ions radiation because carbon ions distribute in a considerably wider region beyond the Bragg-peak due to its strong penetrability (16). The scatter events as a result of energy lost through proton interaction with the nucleus rather than with atomic electrons were well demonstrated with the hydrogen ions radiation (17). These scatters events cause the proton's path to deviate from a straight line, and a lateral fall of 5-8 mm at 10 cm depth was known. The lateral and radial scatters reported in this study are much lower than reported by others (18). The width penetration of hydrogen ions radiation is increased with increasing the acceleration potentials i.e. radiation energy for fixed tissue density and it decreased as the tissue density is increased (19) . It is well known that women with a tumor size more than 1 cm were more likely to have dense breast in mammography compared with a tumor size less than 1 cm (20, 21). Therefore, it is necessary to use high acceleration potential for highly dense breast tissue (i.e. large tumor volume) in order to achieve the full blown Bragg peak. The differences in the skewness and kurtosis of Bragg peaks reflected on the deposition of ionized energy on the tissue as well as it gives a clue for the harmful effect of radiation on the normal tissue. The stopping power of hydrogen ions targeting the atoms in breast tissue is differed from that of carbon ion radiation in respect to the electrons or nuclear stopping power. This observation can explained the

multiple scatters that demonstrated in this study. The fact that the range straggling and multiple scattering are reduced from hydrogen to carbon increases the possibility to accurately deposit only the high linear energy transfer component in the tumor with negligible dose to organs at risk (22). The calculated volume and mass of damaged breast tissue pointed out that the carbon ion radiation is more suitable for superficial and tiny abnormal breast tissue with negligible effect on the normal tissue while the hydrogen ions radiation is suitable for large, deep seated tumors with less acceleration potentials. The relative biological effectiveness of the carbon ions dose (calculated as the ratio of ^{60}Co to proton doses which resulted in the same level of cell survival) deposited in tumor is higher than that reported with hydrogen ions but it carried a potential risk of later onset of secondary cancers (23-25). In this work the relative biological effectiveness of carbon ions is not achieved to the standard of the National Institute of Radiological Sciences which equivalent to 3 at a depth where the dose averaged is 80 keV/micron because the accelerated potentials that are used in this work are less (26). The rational for proton beams for breast tumor results in unparalleled homogeneous dose distributions within complex target volumes, while simultaneously sparing neighboring organs (27). The findings of this study confirmed the advantages of proton therapy for tiny tumors and metastases. It concludes that typical Bragg's peak can be achieved when the density of irradiated tissue , the localization of abnormal tissue , the type of ions radiation and the acceleration potentials are taken collectively in considerations.

Table - 1: Specification of target layers exposed to protons

Tissue			Atomic percent (mass percent)								
	Layer width (A)	Density g/cm^3 (atom/cm^3)	H	C	N	O	Na	S	Cl	K	P
Skin	2x10^7	1.09 (10.56x10^{22})	61.7 (10)	12.9 (25)	2.04 (4.6)	23.1 (59.4)	5.4 (0.199)	5.8 (0.299)	5.3 (0.302)	1.6 (0.100)	- -
Adipose tissue	5x10^7	0.92 (10.35x10^{22})	63.4 (11.9)	28.4 (63.8)	0.305 (0.801)	7.77 (23.2)	1.19 (5.15)	- -	1.79 0.119	- -	- -
Breast density (0.99 g/cm^3)	2x10^8	0.99 (10.39x10^{22})	61.9 (10.8)	24.1 (50.6)	0.941 (2.29)	12.8 (35.7)	0.025 (0.1)	0.018 (0.1)	0.016 (9.89)	-	0.019 (0.102)
Breast density (1.5 g/cm^3)	2x10^8	1.5 (15.75x10^{22})	61.9 (10.8)	24.1 (50.6)	0.941 (2.29)	12.8 (35.7)	0.025 (0.1)	0.018 (0.1)	0.016 (9.89)	-	0.019 (0.102)
Breast density (2.0 g/cm^3)	2x10^8	2.0 (21.0x10^{22})	61.9 (10.8)	24.1 (50.6)	0.941 (2.29)	12.8 (35.7)	0.025 (0.1)	0.018 (0.1)	0.016 (9.89)	-	0.019 (0.102)
Breast density (2.5 g/cm^3)	2x10^8	2.5 (26.25x10^{22})	61.9 (10.8)	24.1 (50.6)	0.941 (2.29)	12.8 (35.7)	0.025 (0.1)	0.018 (0.1)	0.016 (9.89)	-	0.019 (0.102)

A: Armstrong, H: hydrogen, C: carbon, N: nitrogen, O: oxygen, Na: sodium, S: sulphur, Cl: chloride, K: potassium, P: phosphorus

Table -2: The individual data of Bragg's peak generated by hydrogen ions in breast tissue (0.99g/cm^3) at different acceleration potential.

	Longitudinal	Lateral	Radial		Ionization	Vaccancies	Phonens
Breast tissue	Range (straggling)	Range (straggling)	Range (straggling)	Vaccancy ./ ion	Ions (recoil)	Ions (recoil)	Ions (recoil)
Density (0.99g/cm^3) 60 MeV	30.4mm (386 µ)	395 µ (575 µ)	621 µ (511 µ)	228.9	99.96 (0.02)	0 0	0 (0.02)
70 MeV	40.2mm (477 µ)	514 µ (712 µ)	814 µ (657 µ)	258.9	99.96	0 0	0 (0.02)
80 MeV	51.0mm (718 µ)	663 µ (1 mm)	1.04mm (949 µ)	285.9	99.96 (0.02)	0 0	0 (0.02)
90 Mev	63mm (772 µ)	812 µ (1.16mm)	1.26mm (1.04mm)	311.7	99.96 (0.02)	0 0	0 (0.02)

Table -3: The individual data of Bragg's peak generated by hydrogen ions in breast tissue (1.5g/cm^3) at different acceleration potential.

	Long.	Lateral	Radial		Ionization	Vaccancies	Phonens
Breast tissue	Range (straggling)	Range (straggling)	Range (straggling)	Vaccancy./ion	Ions (recoil)	Ions (recoil)	Ions (recoil)
Density (1.5g/cm^3) 60 MeV	26mm (286 µ)	308 µ (479 µ)	485 µ (463 µ)	230.5	99.96 (0.02)	0 0	0 (0.02)
70 MeV	32.4mm (327 µ)	373µ (532 µ)	589 µ (478 µ)	259	99.96	0 0	0 (0.02)
80 MeV	40.8mm (605 µ)	497 µ (727µ)	779 µ (674 µ)	283.9	99.96 (0.02)	0 0	0 (0.02)
90 Mev	40.1mm (672 µ)	715µ (989 µ)	14.6mm (6.41mm)	302.5	99.96 (0.02)	0 0	0 (0.01)

Table -4: The individual data of Bragg's peak generated by hydrogen ions in breast tissue (2 g/cm^3) at different acceleration potential.

	Long.	Lateral	Radial		ionization	vaccancies	phonens		
Mammary gland	Range (strag.)	Range (strag.)	Range (strag.)	Vac./ion	Ions (recoil)	Ions (recoil)	Ions (recoil)	Skewness	kurtosis
Density (2g/cm^3) 60 MeV	23.8mm (220 µ)	264 µ (421 µ)	416 µ (415 µ)	231.4	99.96 (0.02)	0 0	0 (0.02)	-14.2859	607.136
70 MeV	28.7mm (245 µ)	305µ (439 µ)	480 µ (393 µ)	259.7	99.96	0 0	0 (0.02)	-4.4113	132.549
80 MeV	34.1mm (299 µ)	366 µ (545µ)	572 µ (491 µ)	285.9	99.96 (0.02)	0 0	0 (0.02)	-2.0846	39.7743
90 Mev	35.5mm (288 µ)	356 µ (514 µ)	564 µ (473 µ)	313.4	99.96 (0.02)	0 0	0 (0.01)	-1.5526	25.5295

Table -5: The individual data of Bragg's peak generated by hydrogen ions in breast tissue (2.5g/cm^3) at different acceleration potential.

	Long.	Lateral	Radial		ionization	vaccancies	phonens		
Mammary gland	Range (strag.)	Range (strag.)	Range (strag.)	Vac./ion	Ions (recoil)	Ions (recoil)	Ions (recoil)	Skewness	kurtosis
Density (2.5g/cm^3) 60 MeV	22.6mm (182 µ)	238 µ (385 µ)	375 µ (387 µ)	231.9	99.96 (0.02)	0 0	0 (0.02)	-16.7621	775.1576
70 MeV	26.4mm (196 µ)	264µ (380 µ)	410 µ (344 µ)	260.3	99.96	0 0	0 (0.02)	-4.4113	133.1514
80 MeV	30.7mm (237 µ)	307 µ (451µ)	481 µ (402 µ)	286.2	99.96 (0.02)	0 0	0 (0.02)	-1.7378	33.0656
90 Mev	35.5mm (731 µ)	506 µ (723 µ)	794 µ (677 µ)	308.2	99.96 (0.02)	0 0	0 (0.01)	-2.3901	50.1785

Table -6: The individual data of Bragg's peak generated by carbon ions in breast tissue (0.99g/cm^3) at different acceleration potential.

	Long.	Lateral	Radial		ionization	vaccancies	phonens		
Mammary gland	Range (strag.)	Range (strag.)	Range (strag.)	Vac./ion	Ions (recoils)	Ions (recoils)	Ions (recoils)	Skewness	kurtosis
Density (0.99g/cm^3)									
600 MeV	7.48mm (27.4 µ)	31.8 µ (26 µ)	49.9 µ (40 µ)	2912.9	99.94 (0.03)	0 0	0 (0.03)	-4.7695	130.6926
700 MeV	9.83mm (70 µ)	40.2µ (58.8 µ)	63.2 µ (53.9 µ)	3225.3	99.94 (0.03)	0 0	0 (0.02)	-67.2618	5877.178
800 MeV	13mm (47.1 µ)	53.5 µ (79.1µ)	83.2 µ (67.2 µ)	3540	99.95 (0.03)	0 0	0 (0.02)	-0.929	13.0216
900 Mev	15.3mm (80.6 µ)	60.8 µ (85 µ)	95.1 µ (74.5 µ)	3801	99.94 (0.04)	0 0	0 (0.02)	-27.5539	1407.1163

Table- 7: the calculated energy loss of total target (breast tissue 0.99 g/cm^3 density) vacancies /ion irradiated with hydrogen ions (total electrons 25000) or carbon ions (total electrons 10000).

	Energy loss with hydrogen ions (keV)	Energy loss with carbon ions (keV)
Density (0.99g/cm^3) 60 MeV	343.35	
70 MeV	388.35	
80 MeV	428.85	
90 Mev	467.55	
Density (0.99g/cm^3) 600 MeV		4378.5
700 MeV		4837.95
800 MeV		5310
900 MeV		5701.5

Table-8: The stopping power of hydrogen ions targeted each atom in breast tissue at different accelerated potentials

Energy (keV)	Ion	Target	Stopping Electron (keV/μ)	Stopping Nuclear (keV/μ)	Stopping total (keV/μ)	Ion effective charge	Fractional effective charge
60000	H	H	$2.563x10^{5}$	$1.231x10^{-4}$	$2.563x10^{5}$	%1249.885	%1239.965
		C	$6.780x10^{5}$	$8.785x10^{-4}$	$6.780x10^{5}$	%557.293	%552.8697
		N	$2.647x10^{5}$	$3.946x10^{-4}$	$2.647x10^{5}$	519.110	%514.9903
		O	$3.221x10^{5}$	$5.423x10^{-4}$	$3.221x10^{5}$	%490.359	%486.4674
		S	$2.331x10^{5}$	$7.306x10^{-4}$	$2.331x10^{5}$	%362.689	%359.8104
		Cl	$1.932x10^{5}$	$6.144x10^{-4}$	$1.932x10^{5}$	%350.420	%347.6390
		Na	$1.525x10^{5}$	$3.275x10^{-4}$	$1.525x10^{5}$	%428.981	%425.5765
		K	$7.980x10^{4}$	$2.840x10^{-4}$	$7.980x10^{4}$	%334.263	%331.6099
		P	$3.060x10^{5}$	$1.539x10^{-3}$	$3.060x10^{5}$	%274.663	%272.4835
70000	H	H	$2.990x10^{5}$	$1.064x10^{-4}$	$2.990x10^{5}$	%1434.355	%1422.970
		C	$7.910x10^{5}$	$7.629x10^{-4}$	$7.910x10^{5}$	%639.507	%634.4317
		N	$3.088x10^{5}$	$3.428x10^{-4}$	$3.088x10^{5}$	%595.480	%590.7541
		O	$3.758x10^{5}$	4.711x10v	$3.758x10^{5}$	%562.492	%558.0275
		S	$2.720x10^{5}$	$6.354x10^{-4}$	$2.720x10^{5}$	%415.495	%412.1970
		Cl	$2.254x10^{5}$	$5.343x10^{-4}$	$2.254x10^{5}$	%401.668	%398.4798
		Na	$1.779x10^{5}$	$2.845x10^{-4}$	$1.779x10^{5}$	%492.161	%488.2552
		K	$9.310x10^{4}$	$2.471x10^{-4}$	$9.310x10^{4}$	%383.014	%379.9743
		P	$3.570x10^{5}$	$1.340x10^{-3}$	$3.570x10^{5}$	%314.459	%311.9632
80000	H	H	$3.417x10^{5}$	$9.438x10^{-4}$	$3.417x10^{5}$	%1615.052	%1602.2342
		C	$9.040x10^{5}$	$3.034x10^{-4}$	$9.040x10^{5}$	%719.880	%714.1668
		N	$3.529x10^{5}$	$3.034x10^{-4}$	$3.529x10^{5}$	%670.151	%664.8323
		O	$4.294x10^{5}$	$4.170x10^{-4}$	$4.294x10^{5}$	%633.002	%627.9781
		S	$3.108x10^{5}$	$5.628x10^{-4}$	$3.108x10^{5}$	%467.107	%463.3998
		Cl	$2.576x10^{5}$	$4.734x10^{-4}$	$2.576x10^{5}$	%451.736	%463.3998
		Na	$2.033x10^{5}$	$2.520x10^{-4}$	$2.033x10^{5}$	%553.867	%549.4716
		K	$1.064x10^{5}$	$2.189x10^{-4}$	$1.064x10^{6}$	%430.647	%427.2295
		P	$4.080x10^{5}$	$1.188x10^{-3}$	$4.080x10^{5}$	%353.308	%350.5037
90000	H	H	$3.844x10^{5}$	$8.463x10^{-4}$	$3.844x10^{5}$	%1792.253	%1778.0286
		C	$1.017x10^{6}$	$6.060x10^{-4}$	$1.017x10^{6}$	%798.550	%792.2123
		N	$3.970x10^{5}$	$2.723x10^{-4}$	$3.970x10^{5}$	%743.250	%737.3511
		O	$4.831x10^{5}$	$3.744x10^{-4}$	$4.831x10^{5}$	%702.012	%696.4403
		S	$3.497x10^{5}$	$5.057x10^{-4}$	$3.497x10^{5}$	%517.615	513.5071
		Cl	$2.898x10^{5}$	$4.254x10^{-4}$	$2.898x10^{5}$	%500.713	%496.7392
		Na	$2.287x10^{5}$	$2.263x10^{-4}$	$2.287x10^{5}$	%614.212	%609.2589
		K	$1.197x10^{5}$	$2.189x10^{-4}$	$1.197x10^{5}$	%477.247	%473.4589
		P	$4.590x10^{5}$	$1.068x10^{-3}$	$4.590x10^{5}$	%391.282	%388.1767

Table - 9:The stopping power of carbon ions targeted each atom in breast tissue at different accelerated potentials

Energy (keV)	Ion	Target	Stopping Electron (keV/μ)	Stopping Nuclear (keV/μ)	Stopping total (keV/μ)	Ion effective charge	Fractional effective charge
600000	C	H	6.782	$4.570x10^{-3}$	6.782	6	1
		C	$9.031x10^{1}$	$3.617x10^{-2}$	$9.031x10^{1}$	6	1
		N	$4.059x10^{1}$	$1.634x10^{-2}$	$4.059x10^{1}$	6	1
		O	$5.536x10^{1}$	$2.256x10^{-2}$	$5.536x10^{1}$	6	1
		S	$7.299x10^{1}$	$3.102x10^{-2}$	$7.299x10^{1}$	6	1
		Cl	$6.491x10^{1}$	$2.615x10^{-2}$	$6.491x10^{1}$	6	1
		Na	$3.426x10^{1}$	$1.378x10^{-2}$	$3.426x10^{1}$	6	1
		K	$2.944x10^{1}$	$1.212x10^{-2}$	$2.944x10^{1}$	6	1
		P	$1.669x10^{2}$	$6.643x10^{-2}$	$1.669x10^{2}$	6	1
700000	C	H	6	$3.969x10^{-3}$	6.004	6	1
		C	$7.986x10^{1}$	$3.143x10^{-2}$	$7.989x10^{1}$	6	1
		N	$3.592x10^{1}$	$1.420x10^{-2}$	$3.594x10^{1}$	6	1
		O	$4.899x10^{1}$	$1.960x10^{-2}$	$4.901x10^{1}$	6	1
		S	$6.479x10^{1}$	$2.697x10^{-2}$	$6.482x10^{1}$	6	1
		Cl	$5.754x10^{1}$	$2.274x10^{-2}$	$5.746x10^{1}$	6	1
		Na	$3.030x10^{1}$	$1.197x10^{-2}$	$3.032x10^{1}$	6	1
		K	$2.612x10^{1}$	$1.054x10^{-2}$	$2.613x10^{1}$	6	1
		P	$1.483x10^{2}$	$5.781x10^{-2}$	$1.483x10^{1}$	6	1
800000	C	H	5.401	$3.513x10^{-3}$	5.405	6	1
		C	$7.188x10^{1}$	$2.782x10^{-2}$	$7.191x10^{1}$	6	1
		N	$3.236x10^{1}$	$1.257x10^{-2}$	$3.237x10^{1}$	6	1
		O	$4.413x10^{1}$	$1.735x10^{-2}$	$4.415x10^{1}$	6	1
		S	$5.850x10^{1}$	$2.389x10^{-2}$	$5.852x10^{1}$	6	1
		Cl	$5.189x10^{1}$	$2.014x10^{-2}$	$5,191x10^{1}$	6	1
		Na	$2.729x10^{1}$	$1.060x10^{-2}$	$3.730x10^{1}$	6	1
		K	$2.357x10^{1}$	$9.336x10^{-3}$	$2.358x10^{1}$	6	1
		P	$1.340x10^{2}$	$5.124x10^{-2}$	$1.341x10^{2}$	6	1
900000	C	H	4.927	$3.154x10^{-3}$	4.930	6	1
		C	$6.559x10^{1}$	$2.497x10^{-2}$	$6.562x10^{1}$	6	1
		N	$2.954x10^{1}$	$1.128x10^{-2}$	$2.955x10^{1}$	6	1
		O	$4.029x10^{1}$	$1.558x10^{-2}$	$4.031x10^{1}$	6	1
		S	$5.351x10^{1}$	$2.147x10^{-2}$	$5.353x10^{1}$	6	1
		Cl	$4.743x10^{1}$	$1.810x10^{-2}$	$4.745x10^{1}$	6	1
		Na	$2.491x10^{1}$	$9.523x10^{-3}$	$2.492x10^{1}$	6	1
		K	$2.155x10^{1}$	$8.389x10^{-3}$	$2.156x10^{1}$	6	1
		P	$1.227x10^{2}$	$4.606x10^{-2}$	$1.228x10^{2}$	6	1

Table – 10:Effect of proton beam radiation by hydrogen or carbon ions on the breast tissue volume and mass at different range of energies and tissue density.

	Density 1.5 g/cm^3				**Density 2 g/cm^3**				**Density 2.5 g/cm^3**			
	Hydrogen ion		**Carbon ion**		**Hydrogen ion**		**Carbon ion**		**Hydrogen ion**		**Carbon ion**	
MeV	**Volume (cm^3)**	**Mass (g)**	**Volume (cm^3)**	**Mass (g)**	**Volume (cm^3)**	**Mass (g)**	**Volume (cm^3)**	**Mass (g)**	**Volume (cm^3)**	**Mass (g)**	**Volume (cm^3)**	**Mass (g)**
1	**5.087x10^{-12}**	**7.631x10-^{12}**	**1.602x10^{-14}**	**2.4x 10^{-14}**	**2.147x10^{-12}**	**4.295x 10^{-12}**	**6.745x 10^{-15}**	**1.349x 10^{-14}**	**1.089x10^{-12}**	**2.745x10^{-12}**	**3.468x10^{-15}**	**8.670x 10^{-15}**
5	**1.377x10^{-8}**	**2.065x10^{-8}**	**1.147x10^{-13}**	**1.720x10^{-13}**	**5.812x10^{-9}**	**1.162x 10^{-8}**	**4.831x10^{-14}**	**9.663x 10^{-14}**	**2.971x10^{-9}**	**7.427x10^{-9}**	**2.478x10^{-14}**	**6.196x 10^{-14}**
10	**5.674x10^{-7}**	**8.512x10^{-7}**	**4.765x10^{-13}**	**7.148x10^{-13}**	**2.395x10^{-7}**	**4.79x 10^{-7}**	**2.009x10^{-13}**	**4.018x 10^{-13}**	**1.226x10^{-7}**	**3.065x10^{-7}**	**1.029x10^{-13}**	**2.574x 10^{-13}**
20	**2.073x10^{-5}**	**3.11x10^{-5}**	**2.899x10^{-12}**	**4.349x10^{-12}**	**8.727x10^{-6}**	**1.745x 10^{-5}**	**1.223x10^{-12}**	**2.446x 10^{-12}**	**4.468x10^{-6}**	**1.117x10^{-5}**	**6.233x10^{-13}**	**1.558x 10^{-12}**
30	**1.264x10^{-4}**	**1.897x10^{-4}**	**1.152x10^{-11}**	**1.728x10^{-11}**	**7.6x10^{-5}**	**1.520x 10^{-4}**	**4.861x10^{-12}**	**9.722x 10^{-12}**	**3.898x10^{-5}**	**9.745x10^{-5}**	**2.489x10^{-12}**	**6.222x 10^{-12}**
40	**9.086x10^{-4}**	**1.363x10^{-3}**	**3.815x10^{-11}**	**5.722x10^{-11}**	**3.836x10^{-4}**	**7.672x 10^{-4}**	**1.609x10^{-11}**	**3.218x 10^{-11}**	**1.962x10^{-4}**	**4.905x10^{-4}**	**8.258x10^{-12}**	**2.064x 10^{-11}**
50	**3.188x10^{-3}**	**4.782x10^{-3}**	**1.044x10^{-10}**	**1.566x10^{-10}**	**1.344x10^{-3}**	**2.688x 10^{-3}**	**4.399x10^{-11}**	**8.799x 10^{-11}**	**6.884x10^{-4}**	**1.721x10^{-3}**	**2.255x10^{-11}**	**5.637x 10^{-11}**
60	**8.269x10^{-3}**	**1.240x10^{-2}**	**2.314x10^{-10}**	**3.471x10^{-10}**	**3.489x10^{-3}**	**6.978x 10^{-3}**	**9.745x10^{-11}**	**1.949x 10^{-10}**	**1.786x10^{-3}**	**4.465x10^{-3}**	**5.003x10^{-11}**	**1.250x 10^{-10}**
70	**1.810x10^{-2}**	**2.715x10^{-2}**	**4.543x10^{-10}**	**6.815x10^{-10}**	**7.625x10^{-3}**	**1.525x 10^{-2}**	**1.912x10^{-10}**	**3.824x 10^{-10}**	**3.905x10^{-3}**	**9.762x10^{-3}**	**9.791x10^{-11}**	**2.447x 10^{-10}**
80	**4.008x10^{-2}**	**6.013x10^{-2}**	**9.348x10^{-10}**	**1.402x10^{-9}**	**1.695x10^{-2}**	**3.39x 10^{-2}**	**3.941x10^{-10}**	**7.882x 10^{-10}**	**8.664x10^{-3}**	**2.166x10^{-2}**	**2.020x10^{-10}**	**5.050x 10^{-10}**
90	**7.626x10^{-2}**	**1.143x10^{-2}**	**1.695x10^{-9}**	**2.543x10^{-9}**	**3.211x10^{-2}**	**6.422x 10^{-2}**	**7.104x10^{-10}**	**1.420x 10^{-9}**	**1.644x10^{-2}**	**4.11x10^{-2}**	**3.655x10^{-10}**	**9.138x 10^{-10}**

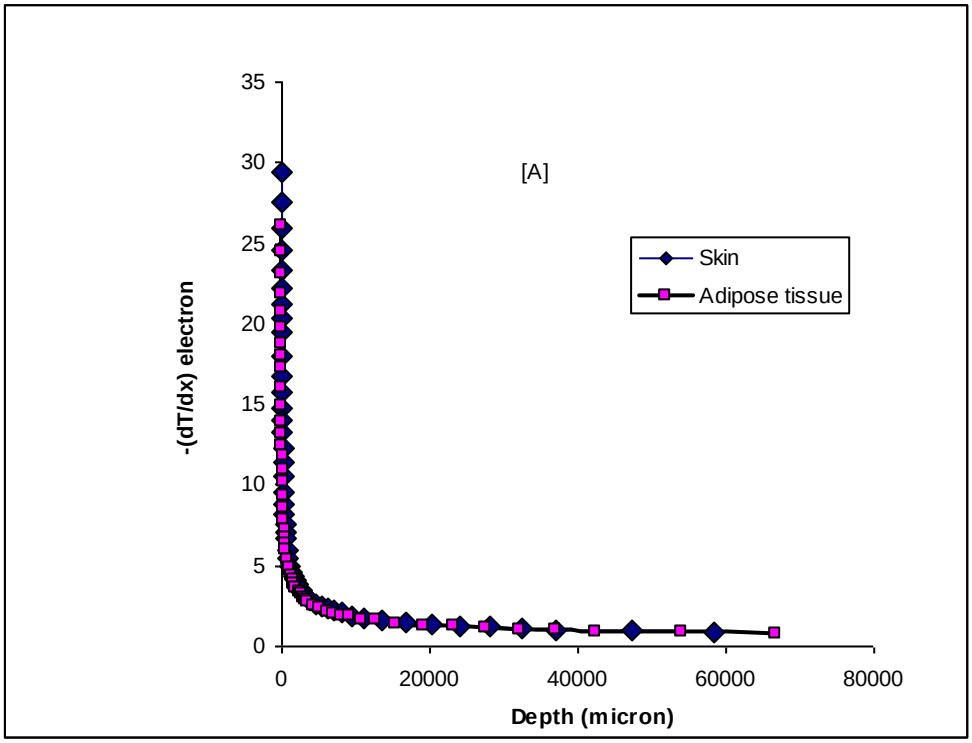

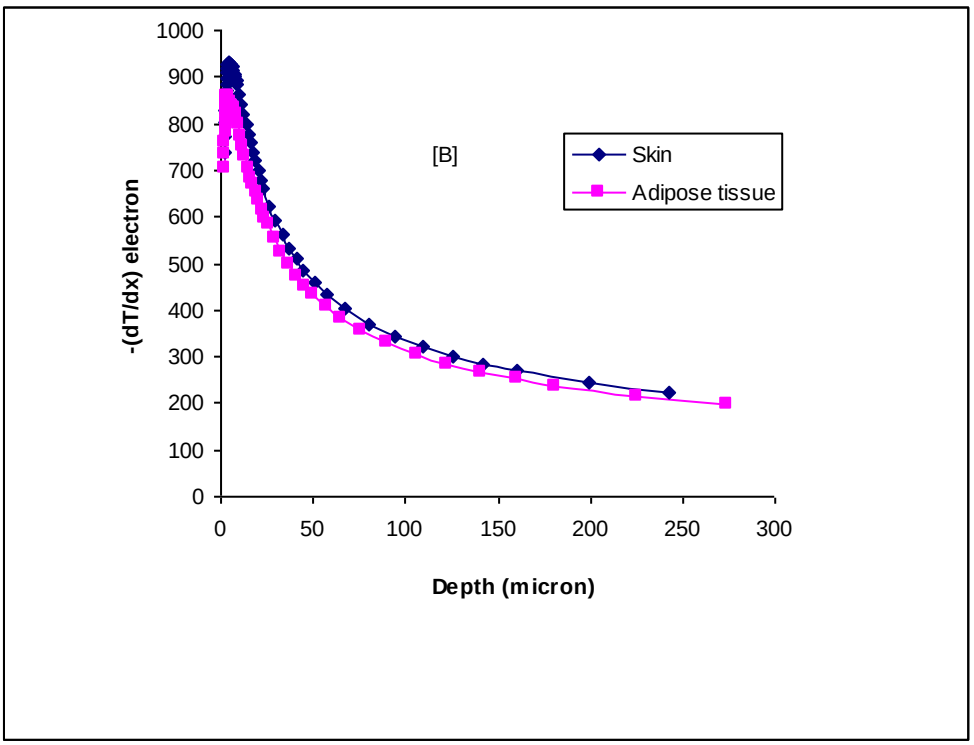

Fig - 1: The stopping power of hydrogen ions [A] and carbon ions [B] in the human skin and adipose tissue

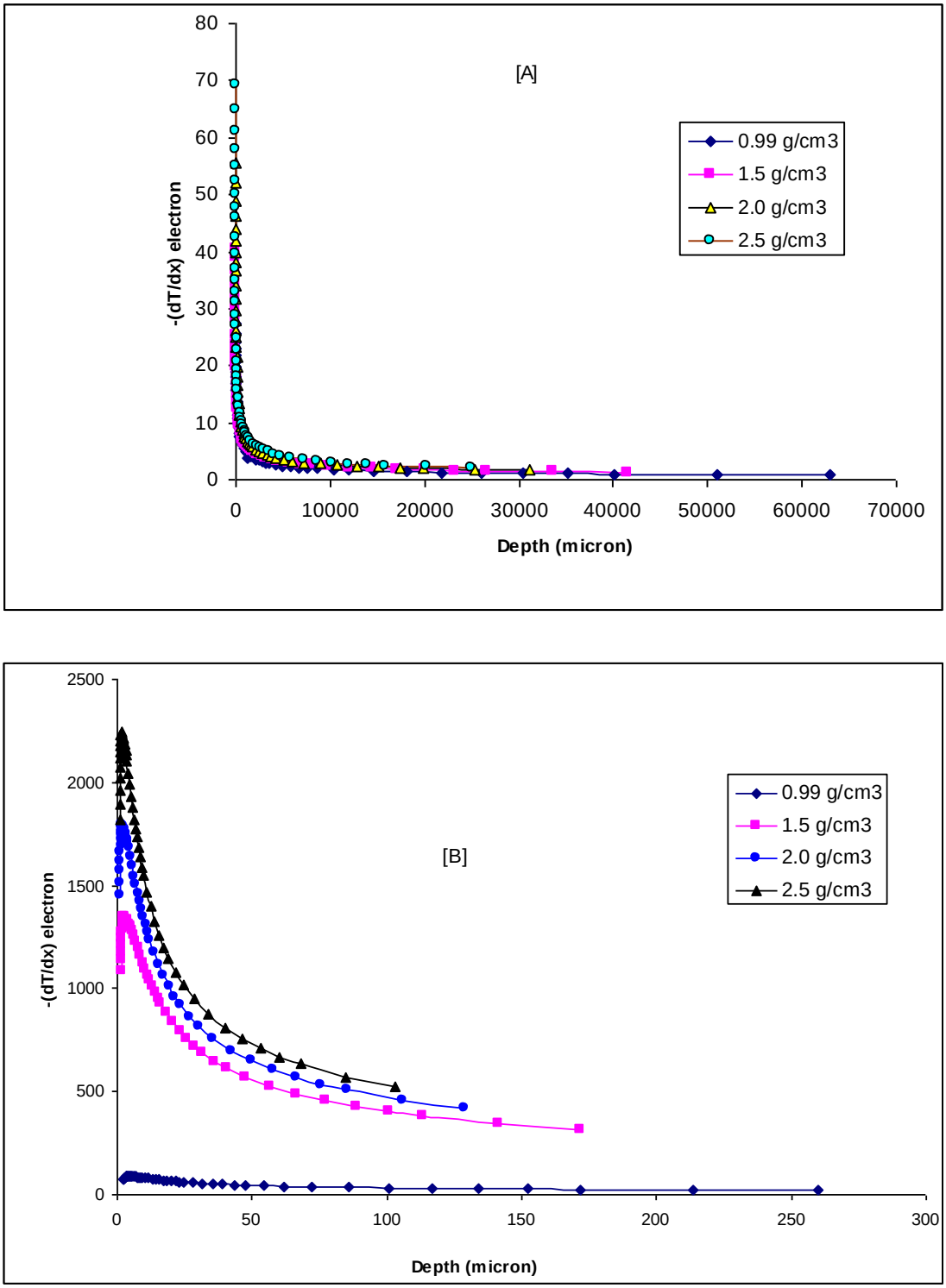

Fig- 2: The stopping power of hydrogen ions [A] and carbon ions [B] in the human breast tissue contained different densities of breast tissues.

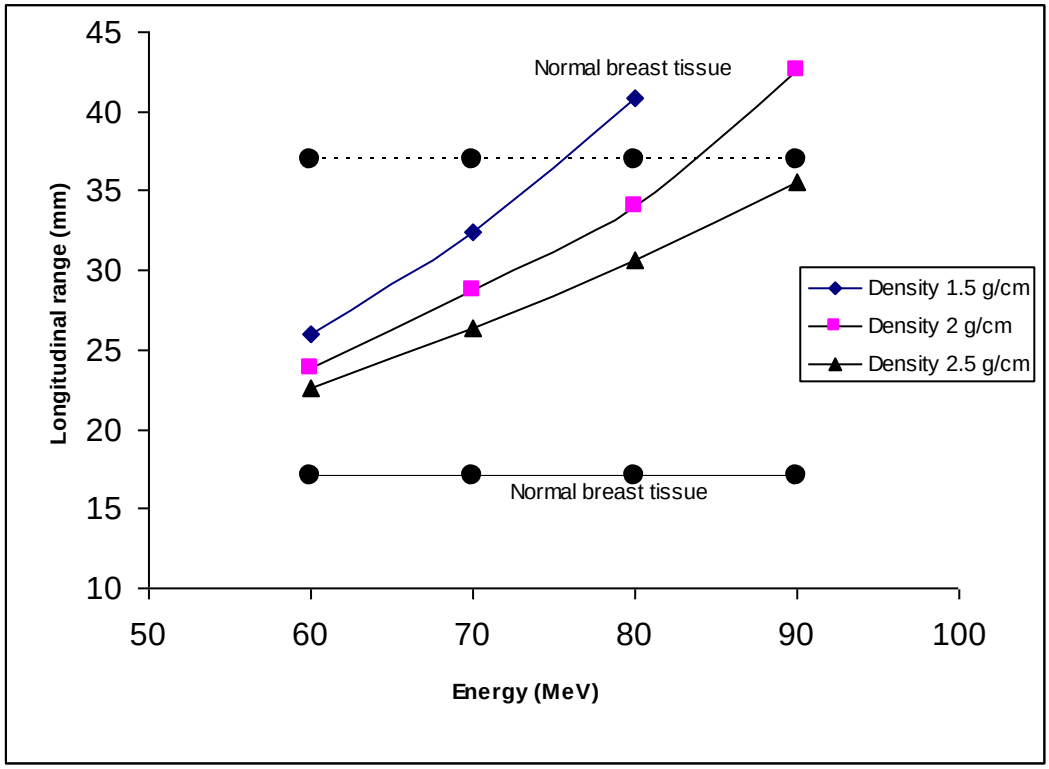
Normal breast tissue
Normal breast tissue
Density 1.5 g/cm
Density 2 g/cm
Density 2.5 g/cm
Longitudinal range (mm)
Energy (MeV)
45
40
35
30
25
20
15
10
50
60
70
80
90
100

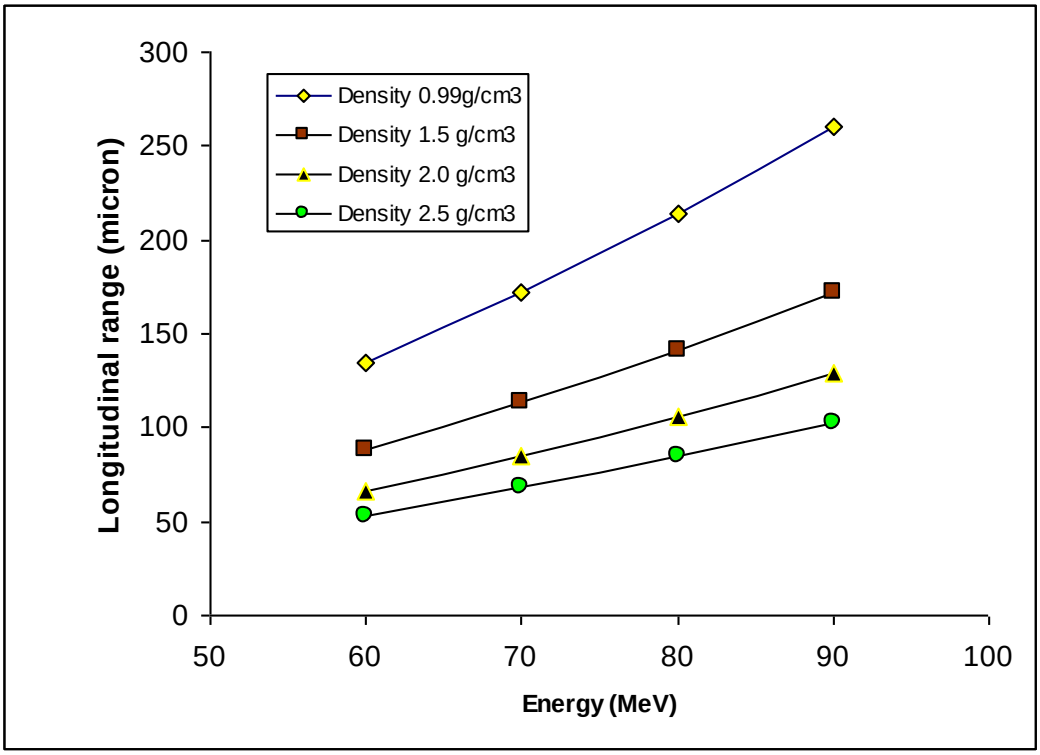
Density 0.99g/cm3
Density 1.5 g/cm3
Density 2.0 g/cm3
Density 2.5 g/cm3
Longitudinal range (micron)
Energy (MeV)
300
250
200
150
100
50
0
50
60
70
80
90
100

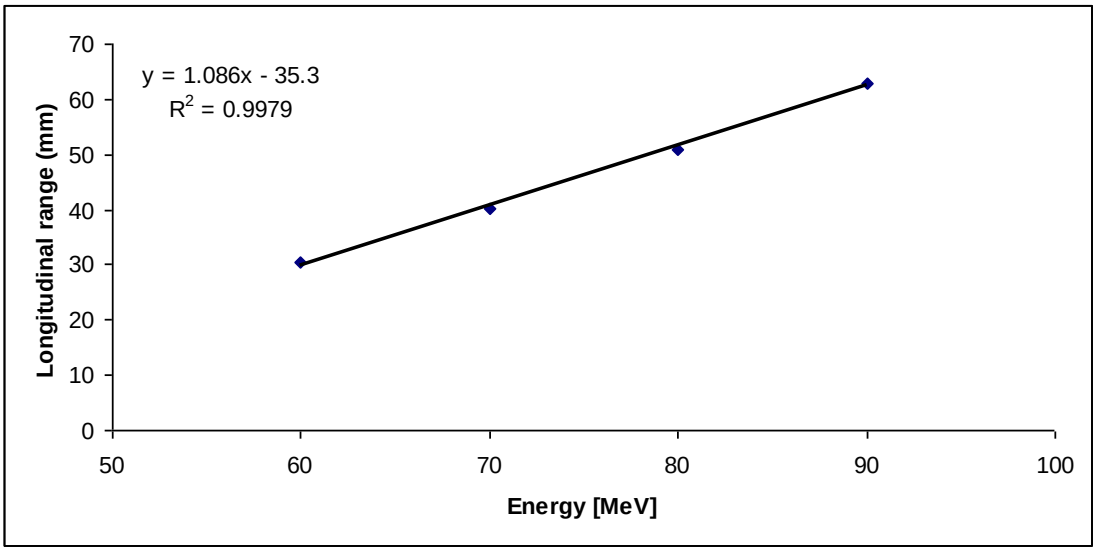

[A]

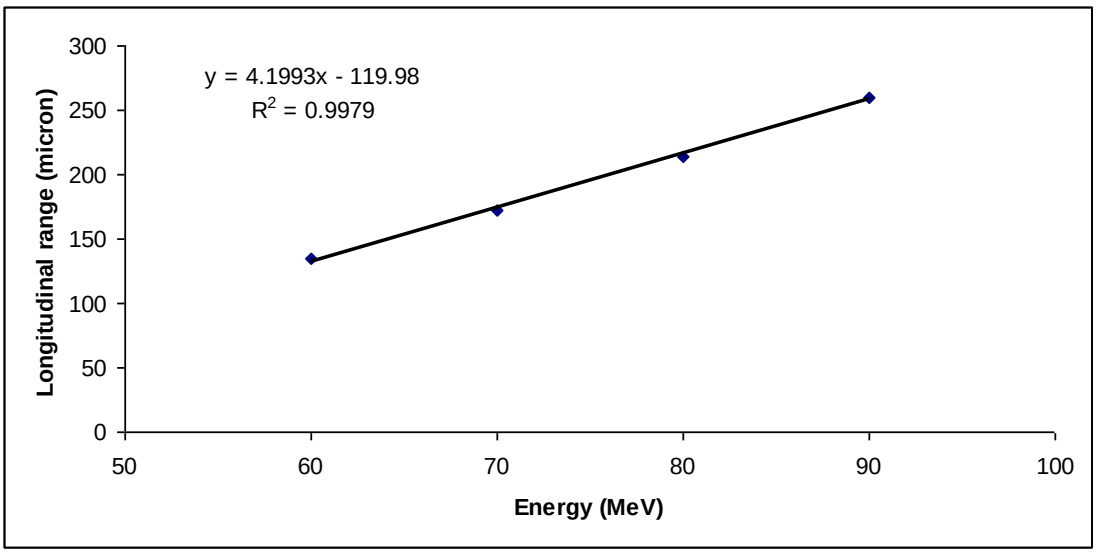

[B]

Fig- 3: Correlation between acceleration potential either with hydrogen ions [A] or carbon ions [B] and longitudinal range

REFERENCES

1. Wilson RR. Radiological use of fast protons. Radiology **47**:487- 491 (1946).
2. Coutrakon G, Bauman M, Lesyna D,Miller D,Nusbaum J,Slater J,Johanning J, Miranda J,DeLuca PM Jr, Siebers J, et al. A prototype beam delivery system for the proton medical accelerator at Loma Linda. Med Phys **18**:1093-1099 (1991).
3. Wagner MS.Automated range compensation for proton therapy.Med Phys **9**:749-752 (1982).
4. Goitein M, Chen F.Beam scanning for heavy charged particle radiotherapy. Med Phys **10**:831-840 (1983).
5. Schulz-Ertner D, Jäkel O, Schlegel W. Radiation therapy with charged particles. Semin Radiat Oncol **16:**249-259 (2006).
6. Fourkal E, Fan J, Veltchev I. Absolute dose reconstruction in proton therapy using PET imaging modality: feasibility study. Phys Med Biol **54**:N217-28(2009)
7. Andisheh B, Brahme A, Bitaraf MA, Mavroidis P, Lind BK.Clinical and radiobiological advantages of single-dose stereotactic light-ion radiation therapy for large intracranial arteriovenous malformations. J Neurosurg , Apr 24(2009).
8. Barker FG 2nd, Butler WE, Lyons S, Cascio E, Ogilvy CS, Loeffler JS, Chapman PH. Dose-volume prediction of radiation-related complications after proton beam radiosurgery for cerebral arteriovenous malformations. J Neurosurg **99**:254-263 (2003).
9. Noël G, Feuvret L, Ferrand R, Mazeron JJ. Treatment with charged particles beams: hydrogen therapy part I: physical basis and clinical experience of treatment with protons. Cancer Radiother **7**:321-339 (2003).
10. Coen JJ, Zietman AL. Proton radiation for localized prostate cancer.Nat Rev Urol **6**:324-330 (2009).
11. Truong MT, Kamat UR, Liebsch NJ, Curry WT, Lin DT, Barker FG 2nd, Loeffler JS, Chan AW. Proton radiation therapy for primary sphenoid sinus malignancies: Treatment outcome and prognostic factors. Head Neck. Jun 17(2009).
12. Bethe H und Ashkin J. In Experimental Nuclear Physics, ed: E. Segre, J Wiley, New York, p253(1953).
13. Wagenaar DJ. Charged particle interactions; Stopping power (1995) http://www.med.harvard.edu/JPNM/physics/nmltd/radprin/sect7/7.1/7_1.2html
14. Ishizaki A, Ishii K, Kanematsu N, Kanai T, Yonai S, Kase Y, Takei Y, Komori M.Development of an irradiation method with lateral modulation of SOBP width using a cone-type filter for carbon ion beams. Med Phys **36**:2222-2227 (2009)
15. Takiguchi Y, Miyamoto T, Nagao K, Kuriyama T. Assessment of the homogeneous efficacy of carbon ions in the spread-out Bragg peak for human lung cancer cell lines. Radiat Med **25**:272-277 (2007).
16. Iwase H, Gunzert-Marx K, Haettner E, Schardt D, Gutermuth F, Kraemer M, Kraft G. Experimental and theoretical study of the neutron dose produced by carbon ion therapy beams. Radiat Prot Dosimetry **126**(1-4):615-618 (2007).
17. Kundrát P. A semi-analytical radiobiological model may assist treatment planning in light ion radiotherapy. Phys Med Biol **52**:6813-6830 (2007).

18. Sawakuchi GO, Titt U, Mirkovic D, Mohan R. Density heterogeneities and the influence of multiple Coulomb and nuclear scatterings on the Bragg peak distal edge of proton therapy beams. Phys Med Biol **53**:4605-4619 (2008).
19. Patyal B. Dosimetry aspects of proton therapy. Technol Cancer Res Treat **6**(4 Suppl):17-23 (2007).
20. Aiello EJ, Buist DSM, White E, Porter PL. Association between mammographic breast density and breast cancer tumor characteristics. Cancer Epidemiol Biomarkers Prev **14**: 662-668 (2005).
21. Heine JJ, Carston MJ, Scott CG, Brandt KR, Wu FF, Pankratz VS, Sellers TA, Vachon CM. An automated approach for estimation of breast density. Cancer Epidemiol Biomarkers Prev **17**:3090-3097 (2008)
22. Kempe J, Gudowska I, Brahme A.Depth absorbed dose and LET distributions of therapeutic 1H, 4He, 7Li, and 12C beams. Med Phys **34**:183-192 (2007).
23. Imaoka T, Nishimura M, Kakinuma S, Hatano Y, Ohmachi Y, Yoshinaga S, Kawano A, Maekawa A, Shimada Y. High relative biologic effectiveness of carbon ion radiation on induction of rat mammary carcinoma and its lack of H-ras and Tp53 mutations. Int J Radiat Oncol Biol Phys **69**:194-203 (2007)
24. Hall EJ. Intensity modulated radiation therapy, protons and the risk of secondary cancer. Int J Radiat Oncol Biol Phys **65**: 1-7 (2006)
25. Weyrather WK, Kraft G. RBE of carbon ions: experimental data and the strategy of RBE calculation for treatment planning. Radiother Oncol **73**: S161-S169 (2004).
26. Matsufuji N, Kanai T, Kanematsu N, Miyamoto T, Baba M, Kamada T, Kato H, Yamada S, Mizoe JE, Tsujii H.Specification of Carbon Ion Dose at the National Institute of Radiological Sciences (NIRS). J Radiat Res (Tokyo) 48 **Suppl A**:A81-86 (2007).
27.Weber DC, Ares C, Lomax AJ, Kurtz JM.Radiation therapy planning with photons and protons for early and advanced breast cancer: an overview. Radiat Oncol **20**; 1:22 (2006).